

# Enhancing metabolic syndrome prediction using fluorine-18 fluorodeoxyglucose positron emission tomography/computed tomography data and machine learning: a comprehensive analysis

Jeonghyun Kang<sup>1</sup>, Jae-Hoon Lee<sup>2</sup>, Hye Sun Lee<sup>3</sup>, Tae Joo Jeon<sup>2</sup>, Young Hoon Ryu<sup>2</sup>

<sup>1</sup>Department of Surgery, Gangnam Severance Hospital, Yonsei University College of Medicine, Seoul, Republic of Korea; <sup>2</sup>Department of Nuclear Medicine, Gangnam Severance Hospital, Yonsei University College of Medicine, Seoul, Republic of Korea; <sup>3</sup>Biostatistics Collaboration Unit, Yonsei University College of Medicine, Seoul, Republic of Korea

Contributions: (I) Conception and design: J Kang, JH Lee; (II) Administrative support: YH Ryu, TJ Jeon; (III) Provision of study materials or patients: J Kang, JH Lee; (IV) Collection and assembly of data: J Kang, TJ Jeon; (V) Data analysis and interpretation: HS Lee, TJ Jeon; (VI) Manuscript writing: All authors; (VII) Final approval of manuscript: All authors.

Correspondence to: Jae-Hoon Lee, MD, PhD. Department of Nuclear Medicine, Gangnam Severance Hospital, Yonsei University College of Medicine, 211 Eonju-Ro, Gangnam-Gu, Seoul 06273, Republic of Korea. Email: docnuke@yuhs.ac.

**Background:** Metabolic syndrome (MetS) is a complex health concern and the incidence of MetS is rising, even among the general population, necessitating effective identification and management strategies. This study aimed to determine if a predictive model using variables from fluorine-18 fluorodeoxyglucose positron emission tomography/computed tomography (FDG PET/CT) and machine learning (ML) could enhance the prediction of MetS.

**Methods:** We retrospectively reviewed the medical records of 1,250 adults who underwent FDG PET/CT for cancer screening between 2014 and 2020. MetS was diagnosed according to the National Cholesterol Education Program Adult Treatment Panel III criteria. The study analyzed standardized uptake values (SUVs), area, and Hounsfield unit (HU) of various body organs from FDG PET/CT and developed a multivariable predictive model for MetS integrating FDG PET/CT variables using least absolute shrinkage and selection operator (LASSO) regression. The performance of a predictive model was assessed using the area under the receiver operating characteristic curve (AUC).

**Results:** The study population comprised 720 men and 530 women with a median age of 54 years, and MetS was present in 26.3% of the subjects. The LASSO regression identified the area of visceral adipose tissue (VAT), mean HU of VAT, mean SUV of VAT, mean HU of skeletal muscle, mean SUV of blood pool, and body mass index as meaningful variables. Our multivariable LASSO model effectively predicted MetS with similar performance in both training and test sets (AUC, 0.792 and 0.828, respectively; P=0.173) and demonstrated superior predictive performance compared to univariable models in the test set (AUC, 0.828)—body mass index (0.794; P=0.017), the area of VAT (0.788; P<0.001), and the mean HU of VAT (0.777; P<0.001).

**Conclusions:** Our findings established the potential of FDG PET/CT, enhanced with ML, in predicting MetS.

**Keywords:** Metabolic syndrome (MetS); positron emission tomography (PET); machine learning (ML)

Submitted Jan 14, 2025. Accepted for publication Jun 18, 2025. Published online Jul 25, 2025. doi: 10.21037/qims-2025-117

View this article at: https://dx.doi.org/10.21037/qims-2025-117

#### Introduction

Metabolic syndrome (MetS) is a complex and significant health concern characterized by a constellation of risk factors that elevate the likelihood of developing cardiovascular diseases, type 2 diabetes mellitus, cancer, and dementia (1-5). The current rise in MetS incidence, even in the general population, presents significant challenges in healthcare management (6). MetS has been defined by multiple organizations with differing criteria, and its application in individuals with established diabetes remains controversial. Although MetS is widely recognized in clinical and research settings, its diagnostic criteria vary slightly across definitions from major organizations, and there is ongoing debate regarding its classification in individuals with pre-existing diabetes (2-4). Nonetheless, given the increasing prevalence and complexity of MetS, accurate identification and risk stratification remain essential for effective management and prevention strategies.

Fluorine-18 fluorodeoxyglucose (FDG) positron emission tomography/computed tomography (PET/ CT), traditionally used for tumor imaging, has also shown promise in assessing MetS. Several studies suggest that metabolic activity in visceral adipose tissue (VAT) and blood pool (BP) uptake may serve as useful imaging biomarkers for MetS (7,8). FDG uptake in the psoas muscle has similarly been linked to early metabolic disturbances (9). Other research has examined VAT and subcutaneous adipose tissue (SAT), demonstrating their associations with obesity-related clinical and biochemical factors (10,11). Moreover, FDG uptake has been shown to differ between metabolically healthy and obese individuals (12). Collectively, these findings indicate that FDG PET/CT can provide valuable insights into the metabolic changes underlying MetS.

However, prior research has not fully utilized the computed tomography (CT) component of PET/CT scans. For instance, the volumes of VAT and SAT, easily measured on CT scans have been thoroughly studied in metabolic disorders, yet previous PET/CT studies have overlooked the integration and comparative analysis of these measurements. Additionally, the effectiveness of models in identifying MetS has been generally limited, with the area under the receiver operating characteristic curve (AUC) typically below 0.8. Integrating a broader range of PET/CT variables into more complex models could enhance predictive accuracy. Moreover, the application of machine learning (ML), which is increasingly prevalent in

data analysis, feature selection, and predictive modeling, can improve predictive capabilities by deriving significant insights from extensive datasets.

Our goal was to assess the practicality and effectiveness of an ML model that utilizes PET/CT data to predict MetS in a generally healthy population. To achieve this, we gathered data on the metabolic activities, volumes, and densities of various organs, including adipose tissue, skeletal muscle, BP, and liver, from FDG PET/CT scans. We then created a multivariable predictive model using the least absolute shrinkage and selection operator (LASSO) and evaluated its ability to predict MetS. We present this article in accordance with the TRIPOD+AI reporting checklist (available at https://qims.amegroups.com/article/view/10.21037/qims-2025-117/rc).

#### **Methods**

## Subject characteristics

Initially, we reviewed the medical records of 1,372 adult subjects who underwent FDG PET/CT for cancer screening from January 2014 to December 2020. The clinical data included sex, body mass index (BMI), waist circumference, systolic and diastolic blood pressure, history of hypertension and diabetes, triglycerides, high-density lipoprotein (HDL) cholesterol, and serum glucose level. Subjects were excluded if they: (I) lacked documented clinical data within 30 days of the PET/CT examination; (II) had a history of malignancy or active inflammatory disease; or (III) had PET/CT data that was unavailable for measurement. Finally, the current study included 1,250 subjects (Figure 1).

This study was conducted in accordance with the Declaration of Helsinki and its subsequent amendments. The study was approved by the institutional review board of Gangnam Severance Hospital (No. 3-2023-0069) and individual consent for this retrospective analysis was waived.

# Determination of MetS

MetS was determined based on the National Cholesterol Education Program-Adult Treatment Panel III criteria (1). MetS was confirmed if any three or more of the following five criteria were met: (I) abdominal obesity, defined as waist circumference >90 cm (Eastern subjects) or 102 cm (Western subjects) in men and >80 cm (Eastern subjects) or 88 cm (Western subjects) in women (13); (II) fasting triglyceride

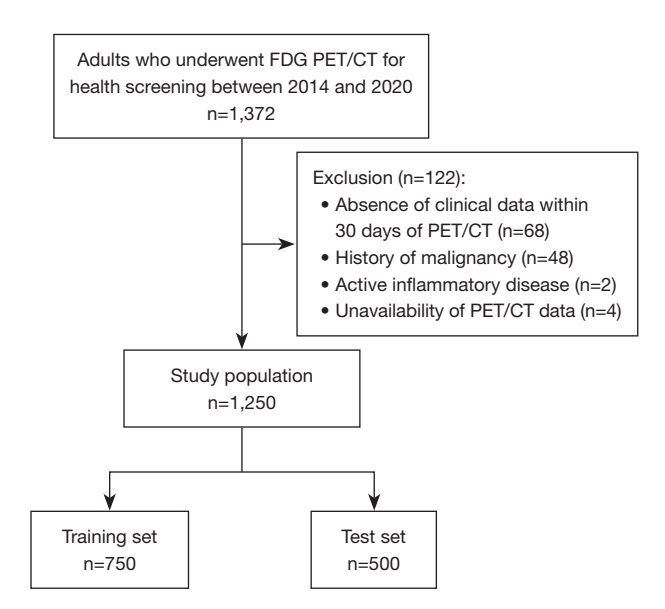


**Figure 1** Study design and flow chart of subject selection. FDG, fluorine-18 fluorodeoxyglucose; PET/CT, positron emission tomography/computed tomography.

concentrations ≥150 mg/dL or a treatment history of dyslipidemia; (III) fasting HDL cholesterol <40 mg/dL in men and <50 mg/dL in women or a treatment history of dyslipidemia; (IV) systolic blood pressure ≥130 mmHg or diastolic blood pressure ≥85 mmHg or treatment for known hypertension; and (V) fasting blood glucose level ≥110 mg/dL or a history of diabetes.

## FDG PET/CT acquisition

All patients fasted for at least 6 hours before FDG PET/CT examination and had blood glucose levels of <140 mg/dL. PET/CT scans were performed 60 min after the intravenous administration of FDG (5.5 MBq/ kg of body weight) using a hybrid PET/CT scanner (Biograph mCT 64, Siemens Healthcare Solutions USA, Inc., Knoxville, TN, USA). A low-dose, non-contrastenhanced CT scan was obtained for attenuation correction with the following parameters: automatic dose modulation with a reference of 120 kVp and 50-80 mAs, slice thickness =3.0 mm, and kernel =B30f. PET data was then acquired from the skull base to the upper thigh at 3 minutes per bed position. PET images were reconstructed onto a 200×200 matrix using three-dimensional ordered subset expectation maximization with point spread function and time-of-flight modeling using two iterations and 21 subsets.

## Image analysis

Three board-certified nuclear medicine physicians, blinded to participants' MetS status, analyzed all FDG PET/CT data employing the open-source LIFEx software (RRID:SCR\_025284; version 7.3.6) (14). In cases of measurement discrepancy, final values were determined by consensus through joint review by the three physicians.

The calculation of the standardized uptake value (SUV) followed this formula: SUV = [decay-corrected activity (kBq) per mL of tissue volume]/[injected FDG activity (kBq) per gram of body mass]. Unless otherwise specified, all SUV values in the main analysis were normalized to body weight (SUV<sub>lw</sub>).

The selection of target organs for image analysis was primarily guided by previous FDG PET/CT research on MetS (7-9). These organs included VAT and SAT, skeletal muscle, liver, spleen, bone marrow, and BP.

Initially, we quantified the maximum and mean SUVs for VAT (VAT SUV $_{max}$  and VAT SUV $_{mean}$ ) and SAT (SAT SUV $_{max}$  and SAT SUV $_{mean}$ ) from PET images (Figure 2A), along with area (cm²) (VAT area and SAT area) and mean Hounsfield unit (HU) values (VAT HU and SAT HU) from CT images using HU threshold range of -190 to -30 HU for the adipose tissue (Figure 2), as previously described (15).

Subsequently, an region of interest (ROI) was meticulously delineated to encompass the skeletal muscles, with a specific focus on the psoas, paraspinal, and abdominal wall muscles. This process involved applying a threshold of -29 to 150 HU within an axial CT image taken at the level of the third lumbar vertebra (*Figure 2B*). Any inner voids within the ROI were filled to ensure the inclusion of the intramuscular fat component. The mean HU of skeletal muscles within the ROI was defined as Muscle HU. The cross-sectional muscle area was then normalized by the square of the height and defined as the skeletal muscle index. The maximum and mean SUVs were measured exclusively for the psoas muscle (Psoas SUV<sub>max</sub> and Psoas SUV<sub>mean</sub>) to replicate the previous research (*Figure 3*) (9).

Finally, the mean SUVs of the liver (Liver SUV<sub>mean</sub>) and spleen (Spleen SUV<sub>mean</sub>) were acquired (*Figure 4A,4B*), as previously described (16). The maximum and mean SUVs of BP (BP SUV<sub>max</sub> and BP SUV<sub>mean</sub>) were also obtained using a spherical ROI placed at the center of the ascending aorta while avoiding FDG uptake in the aortic wall (*Figure 4C*). Additionally, the mean SUV of BM (BM SUV<sub>mean</sub>) was assigned by the mean value of 75% SUV<sub>max</sub> isocontours placed on each lumbar vertebra (*Figure 4D*), as previously described (16).

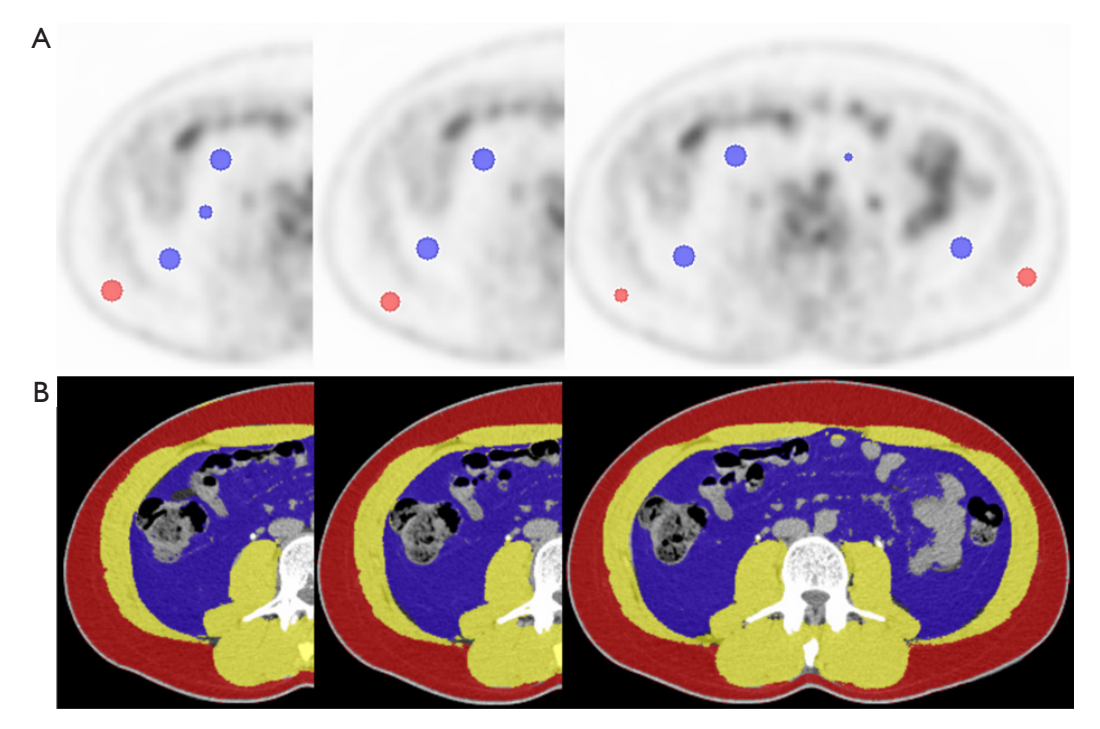


Figure 2 Defining the ROIs for adipose tissues and abdominal skeletal muscles. (A) Circular ROIs (5–15 mm radius) were placed on VAT (blue) and SAT (red) regions of PET images, excluding background contamination, on three consecutive axial PET images at the L3 vertebral level. (B) On three consecutive axial CT images at the L3 vertebral level, the volume of VAT (blue) and SAT (red) were automatically delineated using CT attenuation threshold of –190 to –30 HU, and abdominal skeletal muscles (yellow) using a threshold of –29 to 150 HU. CT, computed tomography; HU, Hounsfield unit; PET, positron emission tomography; ROIs, regions of interest; SAT, subcutaneous adipose tissue; VAT, visceral adipose tissue.

## Predictive model generation using the LASSO regression

The complete study population was randomly divided into training and test sets, maintaining a fixed ratio of 3:2. The predictive model was constructed utilizing the LASSO regression technique within the training set, incorporating 17 FDG PET/CT variables and three clinical variables: sex, age, and BMI. LASSO was chosen for its ability to perform simultaneous variable selection and regularization, thereby reducing overfitting in high-dimensional data. The optimal regularization parameter ( $\lambda$ ) was determined via 10-fold cross-validation within the training set. Model performance was subsequently assessed in the test set using the AUC.

# Lean body mass (LBM)-adjusted SUV analysis

To address the potential confounding effects of body weight on SUVs (17), we conducted an additional analysis using SUVs normalized to LBM (SUL). This normalization was performed using the James formula, which estimates LBM

based on sex, height, and weight as follows (18): for men, LBM =1.10 × weight (kg) – 128 × (weight²/height²); and for women, LBM =1.07 × weight (kg) – 148 × (weight²/height²). The same FDG PET/CT variables were recalculated by converting SUV $_{\rm bw}$  to SUL using the James formula, and then analyzed using the same procedures applied to SUV $_{\rm bw}$ -based data in the previously developed LASSO regression framework, to evaluate whether SUL improved predictive performance compared to conventional SUV $_{\rm bw}$ -based measurements.

## Sex-stratified predictive modeling

To explore potential sex-based variation, we applied the same LASSO regression procedure separately to male and female participants. Each subgroup model was constructed using the identical predictor set and outcome definition as in the main analysis. The discriminative performance of the models was assessed using the AUC, and DeLong's test was used to compare the performance between sexes.

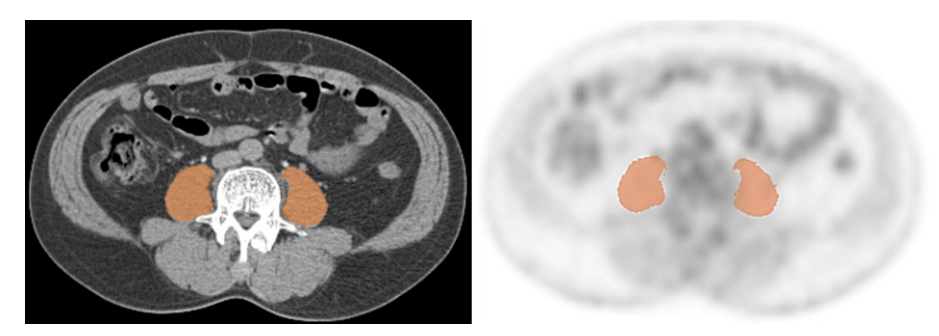


Figure 3 Defining ROI for the psoas muscle. An ROI was defined for the psoas muscle (orange) using a -29 to 150 HU threshold on the CT image (left). This ROI was then transferred to the corresponding PET image to measure FDG uptake of the psoas muscle (right). CT, computed tomography; FDG, fluorine-18 fluorodeoxyglucose; HU, Hounsfield unit; PET, positron emission tomography; ROI, region of interest.

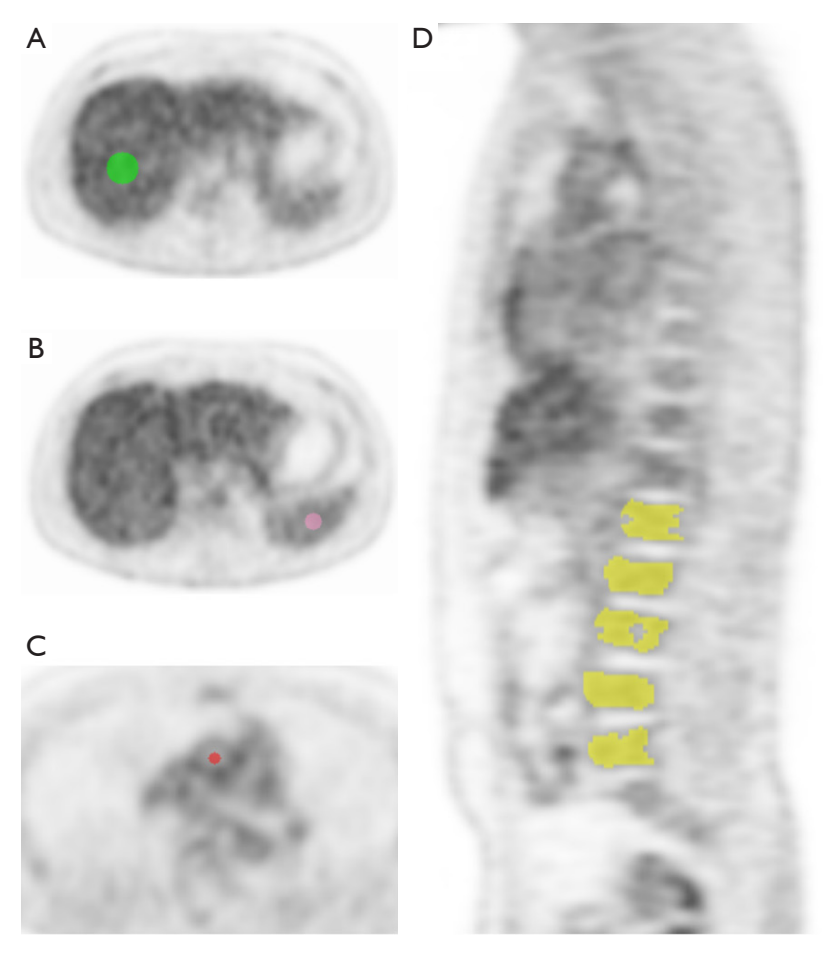


Figure 4 Defining ROIs for the liver, spleen, blood pool, and bone marrow. (A) Liver (green): a spherical ROI (4 cm in diameter) was placed in the right lobe on the PET image. (B) Spleen (pink): a spherical ROI (1.5 cm in diameter) was placed at the center of the spleen. (C) Blood pool (red): a spherical ROI was placed at the center of the ascending aorta, avoiding uptake by the aortic wall on the PET image. (D) Bone marrow (yellow): multiple spheroid ROIs were placed over the lumbar and lower thoracic vertebral bodies on PET images. A 75% SUV<sub>max</sub> isocontour was generated for each ROI, and the FDG uptake within this contour defined the bone marrow SUV. FDG, fluorine-18 fluorodeoxyglucose; PET, positron emission tomography; ROIs, regions of interest; SUV, standardized uptake value; SUV<sub>max</sub>, maximum SUV.

Table 1 Baseline characteristics of study subjects

Characteristics	Value (n=1,250)		
Age (years)	54 [47–60]		
Male	720 (57.6)		
BMI (kg/m²)	24.6 [22.2–27.0]		
Fasting serum glucose (mg/dL)	99 [92–102.8]		
Triglyceride (mg/dL)	114 [83.0–162.8]		
LDL cholesterol (mg/dL)	134 [109.2–158.0]		
HDL cholesterol (mg/dL)	54 [45.0–63.8]		
Total cholesterol (mg/dL)	205 [176–233]		
Systolic blood pressure (mmHg)	122 [113–132]		
Diastolic blood pressure (mmHg)	73 [66–80]		
History of dyslipidemia	217 (17.4)		
History of hypertension	331 (26.5)		
History of diabetes	137 (11.0)		
Metabolic syndrome	329 (26.3)		

Qualitative data are presented as number (percentage); continuous data are presented as median [interquartile range]. BMI, body mass index; HDL, high-density lipoprotein; LDL, low-density lipoprotein.

#### Statistical analysis

Continuous data are reported as mean ± standard deviation or as median with interquartile range (IQR), and comparisons were made using Student's *t*-test or the Mann-Whitney *U* test. Categorical data were presented as counts (percentages) and were compared using the chi-square or Fisher's exact test. The AUC, a performance measure, was presented with a 95% confidence interval (CI). To assess the performance of the developed predictive model, we compared it with other models using DeLong's test for AUCs and decision curve analysis (DCA). A two-sided P value of <0.05 was considered statistically significant. All statistical analyses were conducted using R (version 3.6.3; R Foundation for Statistical Computing, Vienna, Austria).

#### **Results**

#### Study population characteristics

The study population comprised 720 men and 530 women. The median age was 54 years (IQR, 47–60 years), and BMI was 24.6 kg/m<sup>2</sup> (22.2–27.0 kg/m<sup>2</sup>). Three hundred and

twenty-nine participants out of 1,250 (26.3%) satisfied the criteria of MetS. *Table 1* summarizes the demographics of the study population.

There were no significant differences in the clinical and FDG PET/CT variables between the training (n=750) and test sets (n=500) except for SAT area, spleen SUV, BP SUV $_{\rm max}$ , and BP SUV $_{\rm mean}$  (*Table 2*). The incidence of MetS was 25.5% (191/750) in the training and 27.6% (138/500) in the test sets.

## Generation of the predictive model using LASSO regression

In the training set, variable selection for the predictive model was performed using LASSO regression. The variables selected at the minimum lambda value (*Figure 5*) were VAT area (coefficient =0.006), VAT HU (-0.025), VAT SUV $_{\rm mean}$  (-0.244), Muscle HU (-0.029), BP SUV $_{\rm mean}$  (0.289), and BMI (0.072).

## Predictive model evaluation and comparison

The predictive model using LASSO regression showed excellent performance in predicting MetS in both the training set [AUC (95% CI), 0.792 (0.757-0.827)] and the test set [AUC (95% CI), 0.828 (0.791-0.864); P=0.173] (Figure 6). To determine if the multivariable predictive model outperformed univariable predictive models, AUC was calculated for each PET/CT and clinical variable to predict MetS in the test set (*Table 3*). The best three single predictors were BMI [AUC (95% CI), 0.794 (0.753–0.836)], VAT area [AUC (95% CI), 0.788 (0.748–0.828)], and VAT HU [AUC (95% CI), 0.777 (0.735-0.819)], compared with the LASSO predictive model using DeLong's test and DCA. As shown in Figure 7, the LASSO predictive model significantly outperformed BMI (P=0.017), VAT area (P<0.001), and VAT HU (P<0.001) in the test set. In addition, DCA demonstrated that the LASSO multivariable model yielded more net benefits than univariable models.

## LBM-adjusted SUV analysis

The median LBM was 49.56 kg (IQR, 38.62-58.17 kg). The results were comparable to those obtained using SUV<sub>bw</sub>. The variables selected by the LASSO model using SUL were similar to those identified in the SUV<sub>bw</sub>-based model. These included VAT area (coefficient =0.006), VAT HU (-0.037), VAT SUV<sub>mean</sub> (-1.691), Muscle HU (-0.037), BP SUV<sub>mean</sub> (0.402), Spleen SUV (-0.252), and BMI (0.043).

Table 2 Comparison of FDG PET/CT and clinical variables between the training and test sets

Variables	Training (n=750)	Test (n=500)	P value
VAT area (cm²)	138.19 [84.89–196.88]	144.81 [88.72–208.63]	0.167
VAT HU	-94.22 [-98.62 to -87.36]	-94.56 [-98.98 to -88.12]	0.394
VAT SUV <sub>max</sub>	1.35 [1.17–1.56]	1.34 [1.16–1.57]	0.764
VAT SUV <sub>mean</sub>	0.56 [0.49–0.63]	0.56 [0.49–0.64]	0.952
SAT area (cm²)	134.70 [105.09–178.71]	141.74 [108.99–187.32]	0.037
SAT HU	-99.48 [-102.63 to -95.59]	-99.72 [-103.08 to -96.47]	0.081
SAT SUV <sub>max</sub>	0.65 [0.56–0.75]	0.64 [0.55–0.74]	0.454
SAT SUV <sub>mean</sub>	0.31 [0.28–0.35]	0.31 [0.27–0.35]	0.678
Muscle HU	34.96 [28.79–39.21]	34.78 [29.69–38.35]	0.605
L3SMI (cm <sup>2</sup> /m <sup>2</sup> )	43.06 [35.71–49.11]	42.87 [36.32–49.80]	0.606
Psoas SUV <sub>max</sub>	1.12 [1.00–1.26]	1.12 [1.01–1.27]	0.782
Psoas SUV <sub>mean</sub>	0.62 [0.56–0.69]	0.63 [0.58–0.68]	0.369
Liver SUV	2.40 [2.19–2.63]	2.45 [2.22–2.67]	0.089
Spleen SUV	1.97 [1.81–2.13]	2.01 [1.82–2.18]	0.027
BM SUV	1.78 [1.59–2.06]	1.84 [1.60–2.12]	0.159
BP SUV <sub>max</sub>	2.31 [2.11–2.54]	2.34 [2.12–2.62]	0.022
BP SUV <sub>mean</sub>	2.12 [1.93–2.34]	2.14 [1.94–2.42]	0.017
Age (years)	54 [48–60]	54 [47–60]	0.504
Male	434 (57.9)	286 (57.2)	0.861
BMI (kg/m²)	24.50 [22.10–26.90]	24.65 [22.30–27.20]	0.261

Qualitative data are presented as number (percentage); continuous data are presented as median [interquartile range]. BMI, body mass index; BM, bone marrow; BP, blood pool; FDG, fluorine-18 fluorodeoxyglucose; HU, Hounsfield unit; L3SMI, skeletal muscle index measured at the third lumbar vertebra level; max, maximum; PET/CT, positron emission tomography/computed tomography; SAT, subcutaneous adipose tissue; SUV, standardized uptake value; SUV<sub>max</sub>, maximum SUV; SUV<sub>mean</sub>, mean SUV; VAT, visceral adipose tissue.

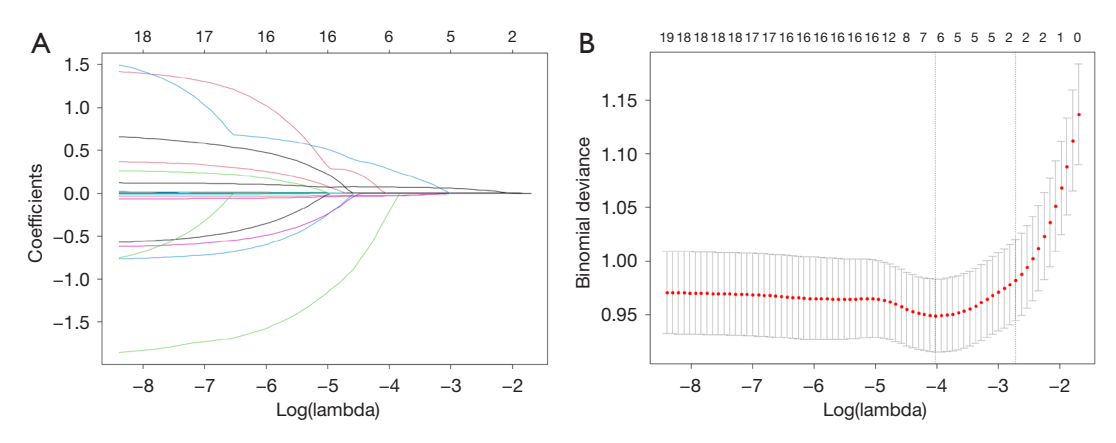


Figure 5 Selection of variables in the training set and definite of linear predictor. (A) Tuning parameters (λ) selection in the LASSO model used 10-fold cross-validation via minimum criteria. (B) LASSO corecipients profile of 20 variables. LASSO, least absolute shrinkage and selection operator.

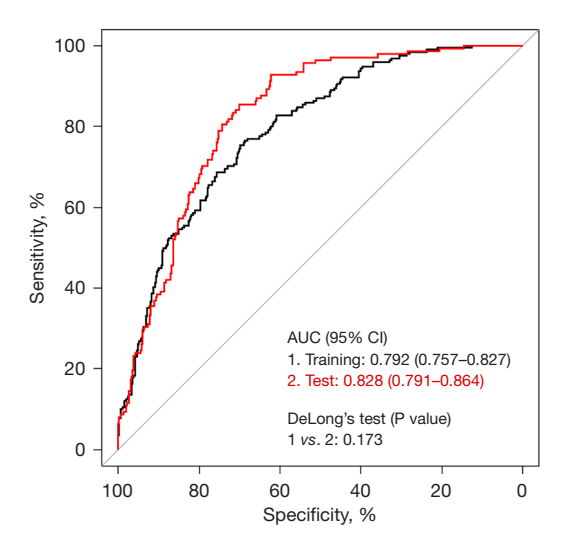


Figure 6 Comparison of AUC of the predictive model in the training and test sets. AUC, area under the curve; CI, confidence interval.

Among the univariable models, BMI, VAT area, and VAT HU demonstrated the strongest predictive performance for MetS. The multivariable model using SUL achieved comparable performance to the SUV<sub>bw</sub>-based model, with an AUC (95% CI) of 0.823 (0.785–0.860) versus 0.828 (0.791–0.864), respectively (P=0.273). Additionally, the SUL-based multivariable model significantly outperformed all univariable models in the test set (*Table 4*) and yielded greater net benefits on DCA (*Figure 8*).

In the sex-stratified analysis, the male-specific model yielded an AUC of 0.804 (95% CI: 0.749–0.859), and the female-specific model achieved an AUC of 0.845 (95% CI: 0.787–0.902). DeLong's test showed no statistically significant difference in performance between the two (P=0.273). Selected features differed partially across sexes, indicating potential biological heterogeneity. Table S1 summarizes these results.

#### **Discussion**

Our principal findings are twofold. First, we reinforced the feasibility of using FDG PET/CT to identify MetS in adults undergoing cancer screening. Second, the use of comprehensive FDG PET/CT variables and ML could enhance the performance of the predictive model. In our analysis, the LASSO predictive model integrated VAT area, VAT HU, VAT SUV<sub>mean</sub>, Muscle HU, BP SUV<sub>mean</sub>, and BMI as significant predictors. Our predictive model not only

**Table 3** Comparison of predictive performance (AUC) between the LASSO multivariable model and univariable models in the training and test sets

Variables	Training (n=750)	Test (n=500)
LASSO model	0.792 (0.757–0.827)	0.828 (0.791-0.864)
VAT area	0.772 (0.735–0.808)	0.788 (0.748-0.828)
VAT HU	0.731 (0.692–0.770)	0.777 (0.735–0.819)
VAT SUV <sub>max</sub>	0.533 (0.486-0.580)	0.555 (0.498–0.612)
VAT SUV <sub>mean</sub>	0.626 (0.584-0.669)	0.634 (0.582-0.687)
SAT area	0.663 (0.618–0.708)	0.686 (0.634-0.738)
SAT HU	0.606 (0.560-0.651)	0.624 (0.569–0.679)
SAT SUV <sub>max</sub>	0.531 (0.483–0.579)	0.570 (0.511-0.629)
SAT SUV <sub>mean</sub>	0.507 (0.461–0.553)	0.542 (0.488–0.597)
Muscle HU	0.641 (0.594–0.687)	0.626 (0.570-0.681)
L3SMI	0.620 (0.574–0.667)	0.562 (0.504–0.620)
Psoas SUV <sub>max</sub>	0.622 (0.579–0.665)	0.585 (0.530-0.640)
Psoas SUV <sub>mean</sub>	0.605 (0.560-0.651)	0.569 (0.510-0.628)
Liver SUV	0.614 (0.568–0.660)	0.599 (0.546-0.653)
Spleen SUV	0.628 (0.583-0.674)	0.631 (0.579–0.684)
BM SUV	0.629 (0.584–0.675)	0.646 (0.592-0.700)
BP SUV <sub>max</sub>	0.654 (0.608–0.699)	0.672 (0.620-0.724)
BP SUV <sub>mean</sub>	0.654 (0.609–0.700)	0.677 (0.625–0.729)
Age	0.548 (0.499–0.598)	0.559 (0.505–0.613)
Sex	0.562 (0.523–0.601)	0.520 (0.471–0.568)
BMI	0.764 (0.726–0.801)	0.794 (0.753–0.836)

Data are presented as AUC with a 95% confidence interval in parentheses. AUC, area under the curve; BMI, body mass index; BM, bone marrow; BP, blood pool; HU, Hounsfield unit; L3SMI, skeletal muscle index measured at the third lumbar vertebra level; LASSO, least absolute shrinkage and selection operator; max, maximum; SAT, subcutaneous adipose tissue; SUV, standardized uptake value; SUV $_{\rm max}$ , maximum SUV; SUV $_{\rm mean}$ , mean SUV; VAT, visceral adipose tissue.

exhibited excellent performance with an AUC of 0.828 in predicting MetS among our large dataset of 1,250 subjects but also significantly outperformed univariable models. Notably, VAT area (AUC =0.788) and VAT HU (0.777) were found to be the most effective single predictors, emphasizing the utility of CT data in PET/CT analysis.

ML methodologies process, train, and analyze extensive datasets to discover underlying patterns and build models

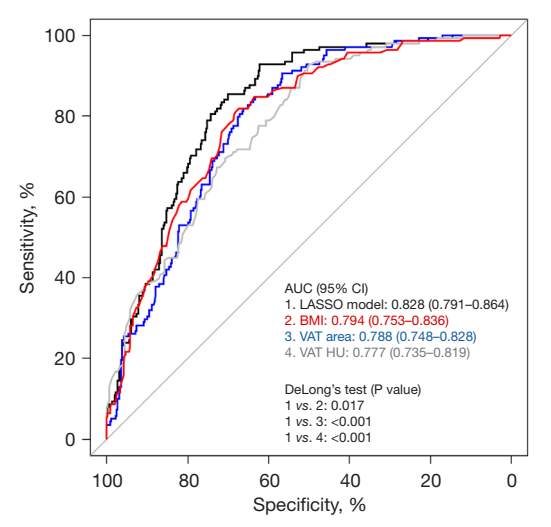


**Figure 7** Comparison of AUC between the LASSO model and three univariable models in the test set. AUC, area under the curve; BMI, body mass index; CI, confidence interval; HU, Hounsfield unit; LASSO, least absolute shrinkage and selection operator; VAT, visceral adipose tissue.

**Table 4** Comparison of predictive performance between the SULbased LASSO model and comparator models

Model	AUC (95% CI)	P value <sup>†</sup>
LASSO (SUL)	0.823 (0.785-0.860)	_
Compared model		
LASSO (SUV <sub>bw</sub> )	0.828 (0.791–0.864)	0.273
BMI (SUL)	0.794 (0.753-0.836)	0.047
VAT area (SUL)	0.788 (0.748-0.828)	0.001
VAT HU (SUL)	0.777 (0.735–0.819)	0.009

<sup>&</sup>lt;sup>†</sup>, P values are derived from DeLong's test comparing the SUL-based LASSO model to each listed comparator. AUC, area under the receiver operating characteristic curve; BMI, body mass index; CI, confidence interval; HU, Hounsfield unit; LASSO, least absolute shrinkage and selection operator; SUL, standardized uptake value normalized to lean body mass; SUV<sub>bw</sub>, standardized uptake value normalized to body weight; VAT, visceral adipose tissue.

for precise classification or prediction. In our research, we employed LASSO regression to analyze a large dataset, identifying VAT area, VAT HU, VAT SUV $_{\rm mean}$ , Muscle HU, BP SUV $_{\rm mean}$ , and BMI as independent predictors for MetS identification. A prior study has indicated the potential of FDG uptake in the psoas muscle as a surrogate marker for metabolic abnormalities (9). The SUV $_{\rm max}$  of the psoas

muscle demonstrated promising predictive performance for MetS with an AUC of 0.779. However, it did not significantly surpass other clinical predictors like BMI in predicting MetS. Another investigation revealed that SUV of BP independently differentiated the metabolically unhealthy group from the metabolically healthy group among obese subjects with modest performance (AUC =0.602) (7). In contrast, our LASSO-based predictive model showed excellent performance with an AUC of 0.828, significantly outperforming other univariable models, including BP SUV, Psoas SUV, and BMI. However, the differences in the study population and measurement technique among the studies need to be acknowledged. Importantly, SUV<sub>mean</sub> is preferred over SUV<sub>max</sub> to represent the relatively homogeneous metabolic change within a target organ because SUV<sub>max</sub> reflects a single pixel and may introduce bias and noise.

Herein, a significant association was observed between reduced VAT SUV<sub>mean</sub> and the presence of MetS, as well as an increase in BP SUV<sub>mean</sub>. While previous research has emphasized the significance of VAT SUV, the specific nature of the correlation between VAT SUV and MetS appears to differ among these studies. Consistent with our findings, prior research has shown a decrease in VAT SUV<sub>mean</sub> among individuals with MetS (8), which could be attributed to factors such as insulin resistance in adipocytes, impaired vascular function, or reduced capillary density, commonly seen in obesity (12). It has been posited that a more metabolically active VAT may act protectively against weight gain (19). In contrast, two other studies have reported higher VAT SUV in MetS patients compared to those without and a positive correlation between adipose tissue metabolic activity and both inflammatory state and metabolic risk (9,11). This inconsistency may be derived from the varied and subjective methodologies in measuring VAT SUV. Currently, there is no standardized or automated approach for accurately segmenting VAT SUVs; hence, most measurements in existing literature rely on manual, visually based assessments. Furthermore, VAT SUV, typically ranging between 0 and 1, is inherently low and falls within a narrow spectrum, making it particularly susceptible to noise, observer variation, and minor group differences that may only be discernible through meticulous image analysis. In this context, measuring FDG uptake of BP might be a more convenient and reproducible method in clinical settings. However, the exact mechanism of increased BP SUV in MetS remains uncertain and potentially complex, although it has been suggested that

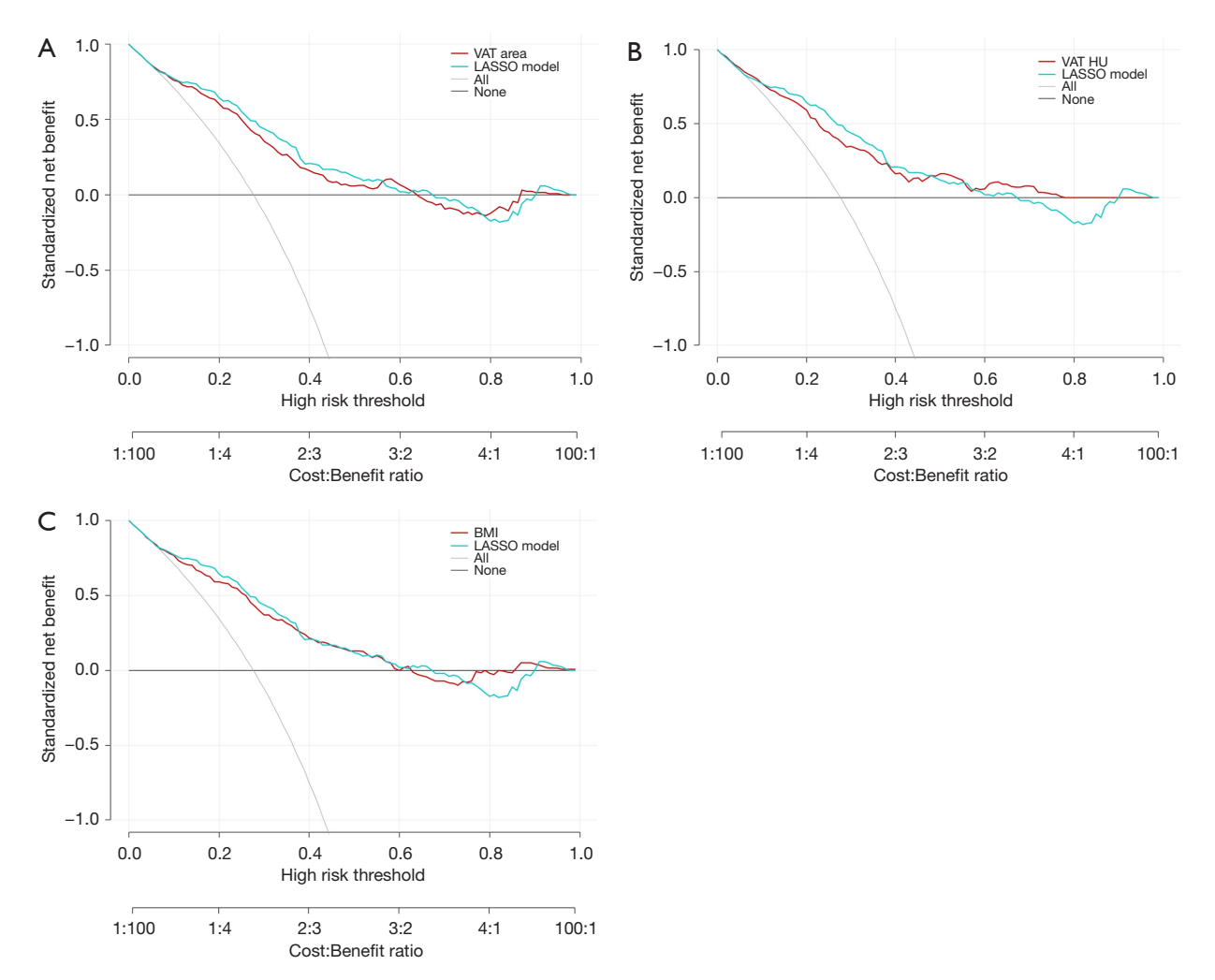


**Figure 8** Decision curve analysis of the LASSO model in comparison to VAT area (A), VAT HU (B), and BMI (C). BMI, body mass index; HU, Hounsfield unit; LASSO, least absolute shrinkage and selection operator; VAT, visceral adipose tissue.

insulin resistance and altered biodistribution in body organs during the development of MetS may contribute to elevated FDG uptake in BP (7,20).

Both VAT HU and Muscle HU were found to be meaningful predictors in MetS risk assessment. While extensive research has focused on the volume of VAT, the study of VAT quality (i.e., VAT HU) has not been as thoroughly explored. Prior studies have demonstrated that fat density, as determined by CT attenuation (HU), was significantly associated with MetS development and progression (21-23). Lower HU values, which suggest fat tissue with larger, lipid-rich adipocytes, were correlated with a heightened risk of MetS (24). This correlation arises because such fat tissue characteristics are strongly associated with adverse cardiometabolic profiles, including

insulin resistance and inflammation, both key elements in MetS pathogenesis (25). However, reduced muscle HU, indicative of myosteatosis, is linked with functional impairments in body organs and an elevated metabolic risk. Longitudinal studies have demonstrated that increased intermuscular adipose tissue, denoted by lower muscle HU values, was independently associated with a heightened risk of developing type 2 diabetes, beyond the contributions of overall and central adiposity and lifestyle risk factors (26,27). Moreover, the accumulation of adipose tissue within skeletal muscle correlated with markers of systemic inflammation and metabolic dysregulation, such as C-reactive protein (28), adiponectin, and leptin (29). This highlights the importance of considering both adipose tissue quality and skeletal muscle density in comprehensive

MetS risk assessments.

Based on the above content, it can be suggested that in the analysis of FDG PET/CT data, CT data offers crucial metabolic information in addition to that provided by PET. While most previous FDG PET/CT studies have focused solely on PET measures, data obtainable from CT, such as VAT area, VAT HU, and Muscle HU, were closely linked to MetS in our study. The integration of this CT information may be a key reason our predictive model exhibited superior performance in identifying MetS compared to existing models. However, one aspect to consider is that although our study demonstrated a high probability of predicting MetS through a comprehensive analysis of FDG PET/CT variables and ML, MetS can typically be diagnosed easily via physical measurements and blood tests. Therefore, the results of this research should be interpreted as providing supplemental information about MetS through image analysis in FDG PET/CT, which was primarily intended for early cancer detection in cancer screenings. Furthermore, the significance of this research extends to providing baseline metabolic data for studies on how changes in FDG uptake in non-tumoral organs observed in PET/CT might affect cancer treatment and prognosis. Additionally, the current manual measurement of body organs can be facilitated with the use of whole-body organ segmentation software utilizing artificial intelligence.

Despite the known limitations of SUV<sub>bw</sub>, such as potential overestimation of metabolic activity in individuals with high adiposity, we retained SUV<sub>bw</sub> as the primary normalization method in this study. This decision was based on several considerations. First, SUV<sub>bw</sub> remains the standard normalization method in clinical and research PET/CT practice, enabling consistency with prior literature and broader applicability across institutions. Second, in our cohort—which consisted exclusively of an East Asian population with relatively low rates of obesity—the impact of excess adiposity on SUV<sub>bw</sub> values is likely to be minimal. Third, the LASSO model using SUL demonstrated comparable predictive performance to the SUV<sub>bw</sub>-based model, with no statistically significant difference in AUC (P=0.273) and nearly identical variable selection. These findings suggest that  $SUV_{bw}$ -based modeling was robust and not meaningfully biased by body composition in this generally healthy population. While SUL offers a theoretical advantage in highly obese or heterogeneous populations, its added complexity and lack of demonstrated benefit in our dataset did not justify replacing SUV<sub>bw</sub> in the primary analysis. Instead, we provided the SUL-based analysis as a complementary result, further supporting the validity and generalizability of our main findings.

Our sex-stratified analysis revealed comparable model performance between men and women, yet partially differing sets of selected predictors. This may reflect known sex-related differences in fat distribution, insulin resistance, and metabolic response, as reported in previous studies (30-34). Although such divergence in feature selection could support sex-specific modeling, the lack of a significant performance gain, combined with added model complexity, led us to retain a unified model. Nonetheless, the findings highlight the biological plausibility of sex-specific metabolic signatures, and suggest directions for future work in larger, more diverse cohorts.

Our study has several limitations. First, it is a crosssectional, single-center investigation, which may limit the generalizability of our findings to broader populations. Heterogeneity in CT scan protocols, including variations in kVp and automatic exposure control across institutions, can affect the image quality and subsequent HU measurements, potentially impacting the performance of our LASSO model. Therefore, further research is needed to validate whether our LASSO model can predict the development or course of MetS in a larger, multi-institutional cohort. Second, we did not perform correlative studies between FDG PET/CT variables and metabolic or inflammatory biomarkers. This omission was because there was significant variability in the availability of metabolic and inflammatory biomarkers within our population, and our primary objective was to determine if the use of ML and PET/CT information could enhance the predictive performance in identifying MetS in a healthy population, compared to previous studies.

#### **Conclusions**

In our research, we employed an ML algorithm integrating FDG PET/CT variables to develop a predictive model aimed at identifying MetS in individuals undergoing FDG PET/CT for cancer screening. The predictive model we devised demonstrated feasibility and excellent performance in predicting MetS within our study cohort. Notably, it outperformed other models that rely on single variables. These findings may emphasize the significant advantage of incorporating CT data from FDG PET/CT scans in evaluating metabolic status.

## **Acknowledgments**

None.

#### **Footnote**

Reporting Checklist: The authors have completed the TRIPOD+AI reporting checklist. Available at https://qims.amegroups.com/article/view/10.21037/qims-2025-117/rc

*Data Sharing Statement:* Available at https://qims.amegroups.com/article/view/10.21037/qims-2025-117/dss

Funding: This study was supported by faculty research grants of Yonsei University College of Medicine (No. 6-2021-0198 to J.H.L.).

Conflicts of Interest: All authors have completed the ICMJE uniform disclosure form (available at https://qims.amegroups.com/article/view/10.21037/qims-2025-117/coif). The authors have no conflicts of interest to declare.

Ethical Statement: The authors are accountable for all aspects of the work in ensuring that questions related to the accuracy or integrity of any part of the work are appropriately investigated and resolved. This study was conducted in accordance with the Declaration of Helsinki and its subsequent amendments. The study was approved by the institutional review board of Gangnam Severance Hospital (No. 3-2023-0069) and individual consent for this retrospective analysis was waived.

Open Access Statement: This is an Open Access article distributed in accordance with the Creative Commons Attribution-NonCommercial-NoDerivs 4.0 International License (CC BY-NC-ND 4.0), which permits the noncommercial replication and distribution of the article with the strict proviso that no changes or edits are made and the original work is properly cited (including links to both the formal publication through the relevant DOI and the license). See: https://creativecommons.org/licenses/by-nc-nd/4.0/.

## References

- Executive Summary of The Third Report of The National Cholesterol Education Program (NCEP) Expert Panel on Detection, Evaluation, And Treatment of High Blood Cholesterol In Adults (Adult Treatment Panel III). JAMA 2001;285:2486-97.
- Kassi E, Pervanidou P, Kaltsas G, Chrousos G. Metabolic syndrome: definitions and controversies. BMC Med 2011;9:48.
- 3. Reaven GM. The metabolic syndrome: time to get off the

- merry-go-round? J Intern Med 2011;269:127-36.
- 4. Grundy SM. Metabolic syndrome update. Trends Cardiovasc Med 2016;26:364-73.
- Mottillo S, Filion KB, Genest J, Joseph L, Pilote L, Poirier P, Rinfret S, Schiffrin EL, Eisenberg MJ. The metabolic syndrome and cardiovascular risk a systematic review and meta-analysis. J Am Coll Cardiol 2010;56:1113-32.
- 6. Saklayen MG. The Global Epidemic of the Metabolic Syndrome. Curr Hypertens Rep 2018;20:12.
- Bang JI, Moon CM, Kim HO, Kang SY, Yoon HJ, Kim BS. Blood pool activity on F-18 FDG PET/CT as a possible imaging biomarker of metabolic syndrome. Sci Rep 2020;10:17367.
- 8. Pahk K, Kim EJ, Lee YJ, Kim S, Seo HS. Characterization of glucose uptake metabolism in visceral fat by 18 F-FDG PET/CT reflects inflammatory status in metabolic syndrome. PLoS One 2020;15:e0228602.
- Kim JY, Jun DW, Choi J, Nam E, Son D, Choi YY. Psoas muscle fluorine-18-labelled fluoro-2-deoxy-d-glucose uptake associated with the incidence of existing and incipient metabolic derangement. J Cachexia Sarcopenia Muscle 2019;10:894-902.
- Monteiro AM, Ferreira G, Duarte H. Metabolic Activity in the Visceral and Subcutaneous Adipose Tissues by FDG-PET/CT in Obese Patients. Acta Med Port 2017;30:813-7.
- 11. Tahara N, Yamagishi S, Kodama N, Tahara A, Honda A, Nitta Y, Igata S, Matsui T, Takeuchi M, Kaida H, Kurata S, Abe T, Fukumoto Y. Clinical and biochemical factors associated with area and metabolic activity in the visceral and subcutaneous adipose tissues by FDG-PET/CT. J Clin Endocrinol Metab 2015;100:E739-47.
- 12. Oliveira AL, Azevedo DC, Bredella MA, Stanley TL, Torriani M. Visceral and subcutaneous adipose tissue FDG uptake by PET/CT in metabolically healthy obese subjects. Obesity (Silver Spring) 2015;23:286-9.
- 13. Kwon HS, Park YM, Lee HJ, Lee JH, Choi YH, Ko SH, Lee JM, Kim SR, Kang SY, Lee WC, Ahn MS, Noh JH, Kang JM, Kim DS, Yoon KH, Cha BY, Lee KW, Kang SK, Son HY. Prevalence and clinical characteristics of the metabolic syndrome in middle-aged Korean adults. Korean J Intern Med 2005;20:310-6.
- 14. Nioche C, Orlhac F, Boughdad S, Reuzé S, Goya-Outi J, Robert C, Pellot-Barakat C, Soussan M, Frouin F, Buvat I. LIFEx: A Freeware for Radiomic Feature Calculation in Multimodality Imaging to Accelerate Advances in the Characterization of Tumor Heterogeneity. Cancer Res 2018:78:4786-9.
- 15. Lee JH, Kim S, Lee HS, Park EJ, Baik SH, Jeon TJ, Lee

- KY, Ryu YH, Kang J. Different prognostic impact of glucose uptake in visceral adipose tissue according to sex in patients with colorectal cancer. Sci Rep 2021;11:21556.
- Lee JH, Lee HS, Kim S, Park EJ, Baik SH, Jeon TJ, Lee KY, Ryu YH, Kang J. Prognostic significance of bone marrow and spleen (18)F-FDG uptake in patients with colorectal cancer. Sci Rep 2021;11:12137.
- Sarikaya I, Albatineh AN, Sarikaya A. Revisiting Weight-Normalized SUV and Lean-Body-Mass-Normalized SUV in PET Studies. J Nucl Med Technol 2020;48:163-7.
- 18. James WPT. Research on obesity. Nutrition Bulletin 1977;4:187-90.
- Goncalves MD, Green-McKenzie J, Alavi A, Torigian DA. Regional Variation in Skeletal Muscle and Adipose Tissue FDG Uptake Using PET/CT and Their Relation to BMI. Acad Radiol 2017;24:1288-94.
- 20. Zeyda M, Stulnig TM. Obesity, inflammation, and insulin resistance—a mini-review. Gerontology 2009;55:379-86.
- Baba S, Jacene HA, Engles JM, Honda H, Wahl RL. CT Hounsfield units of brown adipose tissue increase with activation: preclinical and clinical studies. J Nucl Med 2010;51:246-50.
- 22. Lee YS, Hong N, Witanto JN, Choi YR, Park J, Decazes P, Eude F, Kim CO, Chang Kim H, Goo JM, Rhee Y, Yoon SH. Deep neural network for automatic volumetric segmentation of whole-body CT images for body composition assessment. Clin Nutr 2021;40:5038-46.
- 23. Rosenquist KJ, Massaro JM, Pedley A, Long MT, Kreger BE, Vasan RS, Murabito JM, Hoffmann U, Fox CS. Fat quality and incident cardiovascular disease, all-cause mortality, and cancer mortality. J Clin Endocrinol Metab 2015;100:227-34.
- 24. Lee JJ, Pedley A, Hoffmann U, Massaro JM, Keaney JF Jr, Vasan RS, Fox CS. Cross-Sectional Associations of Computed Tomography (CT)-Derived Adipose Tissue Density and Adipokines: The Framingham Heart Study. J Am Heart Assoc 2016;5:e002545.
- 25. Chait A, den Hartigh LJ. Adipose Tissue Distribution, Inflammation and Its Metabolic Consequences, Including

Cite this article as: Kang J, Lee JH, Lee HS, Jeon TJ, Enhancing metabolic syndrome prediction using fluorine-18 fluorodeoxyglucose positron emission tomography/computed tomography data and machine learning: a comprehensive analysis. Quant Imaging Med Surg 2025;15(8):7524-7536. doi: 10.21037/qims-2025-117

- Diabetes and Cardiovascular Disease. Front Cardiovasc Med 2020;7:22.
- Miljkovic I, Kuipers AL, Cvejkus R, Bunker CH, Patrick AL, Gordon CL, Zmuda JM. Myosteatosis increases with aging and is associated with incident diabetes in African ancestry men. Obesity (Silver Spring) 2016;24:476-82.
- Tanaka M, Okada H, Hashimoto Y, Kumagai M, Nishimura H, Fukui M. Low-attenuation muscle is a predictor of diabetes mellitus: A population-based cohort study. Nutrition 2020;74:110752.
- 28. Miljkovic I, Kuipers AL, Kammerer CM, Wang X, Bunker CH, Patrick AL, Wheeler VW, Kuller LH, Evans RW, Zmuda JM. Markers of inflammation are heritable and associated with subcutaneous and ectopic skeletal muscle adiposity in African ancestry families. Metab Syndr Relat Disord 2011;9:319-26.
- Vella CA, Cushman M, Van Hollebeke RB, Allison MA. Associations of Abdominal Muscle Area and Radiodensity with Adiponectin and Leptin: The Multiethnic Study of Atherosclerosis. Obesity (Silver Spring) 2018;26:1234-41.
- 30. Mauvais-Jarvis F, Bairey Merz N, Barnes PJ, Brinton RD, Carrero JJ, DeMeo DL, De Vries GJ, Epperson CN, Govindan R, Klein SL, Lonardo A, Maki PM, McCullough LD, Regitz-Zagrosek V, Regensteiner JG, Rubin JB, Sandberg K, Suzuki A. Sex and gender: modifiers of health, disease, and medicine. Lancet 2020;396:565-82.
- 31. Regitz-Zagrosek V. Sex and gender differences in health. Science & Society Series on Sex and Science. EMBO Rep 2012;13:596-603.
- 32. Fahed G, Aoun L, Bou Zerdan M, Allam S, Bou Zerdan M, Bouferraa Y, Assi HI. Metabolic Syndrome: Updates on Pathophysiology and Management in 2021. Int J Mol Sci 2022;23:786.
- 33. Liu KA, Mager NA. Women's involvement in clinical trials: historical perspective and future implications. Pharm Pract (Granada) 2016;14:708.
- 34. Peters SAE, Woodward M. Sex Differences in the Burden and Complications of Diabetes. Curr Diab Rep 2018;18:33.